CFD simulation of horizontal oil-water flow with matched density and medium viscosity ratio in different flow regimes

Jing Shi, Mustapha Gourma, Hoi Yeung

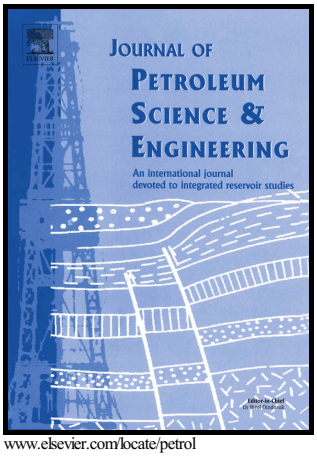

www.elsevier.com/locate/petrol

PII: S0920-4105(17)30067-0
DOI: http://dx.doi.org/10.1016/j.petrol.2017.01.022
Reference: PETROL3831

To appear in: *Journal of Petroleum Science and Engineering*

Received date: 5 August 2016
Revised date: 14 December 2016
Accepted date: 9 January 2017

Cite this article as: Jing Shi, Mustapha Gourma and Hoi Yeung, CFD simulation of horizontal oil-water flow with matched density and medium viscosity ratio in different flow regimes, *Journal of Petroleum Science and Engineering* http://dx.doi.org/10.1016/j.petrol.2017.01.022

Journal of Petroleum Science and Engineering, Vol. 151, March 2017, pp. 373-383
DOI:10.1016/j.petrol.2017.01.022

CFD simulation of horizontal oil-water flow with matched density and medium viscosity ratio in different flow regimes

Jing Shi*, Mustapha Gourma, Hoi Yeung

Oil and Gas Engineering Centre, School of Energy, Environment and Agrifood, Cranfield University, Cranfield MK43 0AL, UK

*Corresponding author. jingshi1988@gmail.com

Abstract

Simulation of horizontal oil-water flow with matched density and medium viscosity ratio (μ_o/μ_w=18.8) in several different flow regimes (core annular flow, oil plugs/bubbles in water and dispersed flow) was performed with the CFD package FLUENT in this study. The volume of fluid (VOF) multiphase flow modeling method in conjunction with the SST *k-ω* scheme was applied to simulate the oil-water flow. The influences of the turbulence schemes and wall contact angles on the simulation results were investigated for a core annular flow (CAF) case. The SST *k-ω* turbulence scheme with turbulence damping at the interface gives better predictions than the standard *k-ε* and RNG *k-ε* models for the case under consideration. The flow regime of density-matched oil-water flow with medium viscosity ratio, or more generally speaking, the flow regime of fluids where the surface tension is playing a prevailing role is sensitive to the wall contact angle. Simulation results were compared with experimental counterparts. Satisfactory agreement in the prediction of flow patterns were obtained for CAF and oil plugs/bubbles in water. The simulation results also demonstrated some detailed flow characteristics of CAF with relatively low-viscosity oil (oil viscosity one order higher than the water viscosity in the present study compared to the extensively studied CAF with oil viscosity being two to three orders higher than the water viscosity). Different from the velocity profiles of high-viscosity oil CAF where there is sharp change in the velocity gradient at the phase interface with velocity across the oil core being roughly flat, there is no sharp change in the velocity gradient at the phase interface for CAF with relatively low-viscosity oil.

Keywords

Oil-water; Computational fluid dynamics (CFD); Volume of fluid (VOF); Flow pattern; Core annular flow (CAF)

Symbols used

A	[m^2]	cross-sectional area of the pipe
A_i	[m^{-1}]	interface area density
A_w	[m^2]	cross-sectional area occupied by water
B	[-]	turbulence damping factor, 10
d	[m]	internal pipe diameter
d_{we}	[m]	hydraulic diameter of the water phase
D_ω	[kg $m^{-2}s^{-2}$]	cross-diffusion term in the specific dissipation rate equation
F	[kg $m^{-2}s^{-2}$]	external body force per unit volume
g	[m s^{-2}]	gravitational acceleration
G_k	[kg $m^{-1}s^{-3}$]	production of turbulent kinetic energy
G_ω	[kg $m^{-2}s^{-2}$]	generation term of the turbulence specific dissipation rate
H_w	[-]	water holdup
I	[-]	turbulence intensity
k	[m^2 s^{-2}]	kinetic energy of turbulence
m	[-]	empirical coefficient in the model of turbulent flow velocity profile
n	[m^{-1}]	surface normal vector
$\hat{\mathrm{n}}$	[m^{-1}]	unit surface normal vector
$\hat{\mathrm{n}}_{\mathrm{wl}}$	[m^{-1}]	unit vector normal to the wall
p	[N m^{-2}]	pressure
r	[m]	radial position
R	[m]	radius of pipe
S_ω	[kg $m^{-2}s^{-2}$]	source term for reduction of the destruction term in the specific dissipation rate equation

t	[s]	time
$\hat{t}_{wl}$	[m^{-1}]	unit vector tangential to the wall
u	[m s^{-1}]	velocity
U	[m s^{-1}]	average velocity
U_m	[m s^{-1}]	mixture average velocity
U_{max}	[m s^{-1}]	mixture maximum velocity
U_{so}	[m s^{-1}]	superficial oil velocity
U_{sw}	[m s^{-1}]	superficial water velocity
z	[m]	longitudinal position from the junction
Y_k	[kg $m^{-1}s^{-3}$]	dissipation of turbulent kinetic energy
Y_ω	[kg $m^{-2}s^{-2}$]	dissipation term for the turbulence specific dissipation rate

Greek letters

α	[-]	volume fraction
β	[-]	closure coefficient in turbulence damping term, 0.075
θ_{wl}	[°]	angle between the wall and the tangent to the interface at the wall
κ	[m^{-1}]	interface curvature
μ	[kg $m^{-1}s^{-1}$]	molecular viscosity
μ_t	[kg $m^{-1}s^{-1}$]	turbulent viscosity
ρ	[kg m^{-3}]	density
σ	[N m^{-1}]	surface tension coefficient
σ_k	[-]	Prandtl number for kinetic energy equation
σ_ω	[-]	Prandtl number for specific dissipation rate equation
φ	[-]	interface area density
ω	[s^{-1}]	specific dissipation rate
ω_ω	[s^{-1}]	additional specific dissipation rate term in the interface turbulence

damping model

Δn	[m]	grid size in the interface region

Subscripts

i	[-]	interface
k	[-]	kinetic energy equation
o	[-]	oil
q	[-]	phase index
t	[-]	turbulence
w	[-]	water
wl	[-]	wall
ω	[-]	specific dissipation rate equation

1. Introduction

Flows of two immiscible liquids are encountered in a diverse range of processes, and particularly in the petroleum industry, where oil and water are often produced and transported together. During the concurrent flow of oil and water in a pipe, the deformable interface of the two fluids can attain a variety of characteristic configurations known as flow regimes. Accurate prediction of oil-water flow characteristics such as the flow regime, water holdup, and pressure gradient is of importance for engineering design and operation.

Computational fluid dynamics (CFD) is a useful tool which can give insight and foresight of flow behaviors. It is becoming increasingly popular with advancement of the computer technology. Some dedicated in-house CFD codes have been developed in order to investigate the stability of CAF flows. Ooms et al. (1984) numerically modelled highly viscous oil CAF by assuming the oil core being solid. The model was based on the hydrodynamic lubrication theory and numerically solved with the shape of the wave being empirical input. Bai et al. (1996) conducted numerical calculation of laminar CAF of liquids with same density under assumptions of axisymmetric interfacial waves and a solid oil core. Ko et al. (2002) extended the numerical simulation of Bai et al. (1996) to turbulent case by adopting the SST *k-ω* model. Li and Renardy (2000) developed a semi-implicit VOF solver to study vertical core annular flow at low Reynolds number. Amongst many theoretical findings from the aforementioned studies is the importance

of interfacial waves in the levitation of the core. It is noted that all the aforementioned studies focus on high-viscosity oil CAF (oil viscosity 2 to 3 orders higher than the water viscosity) and most of the models assume that the high-viscosity oil core being solid-like to simplify the mathematical description of the CAF. CAF is with relatively low-viscosity oil has received little attention. For low-viscosity oil-water flow, CAF would develop when densities of fluids are matched. In density-matched CAF with relatively low-viscosity oil, some interesting flow characteristics different from the extensively studies high-viscosity oil CAF would show as the influence of gravitational force disappear, the viscous force is not as dominant as in high-viscosity oil-water flow, while at the same time the interfacial tension and/or the inertia play more prevailing roles depending on the flow conditions. The flow characteristics of density-matched CAF with relatively low-viscosity oil has not been sufficiently discussed.

In engineering applications, the commercial CFD packages are gaining increasing popularity. The general CFD codes ease the heavy work on coding and could provide reasonable results if the simulations are appropriately set up. A good understanding on the CFD models and numerical theories is essential to perform CFD simulations correctly. In addition, investigations on the suitability of the general built-in models to particular problems are required. One of the most important decisions that have to be made in any numerical study of fluid flow is the choice of the turbulence model as it bears a substantial effect on the accuracy of the result. A large number of studies in the literature have reported assessment of different turbulence models for single phase flow, particularly in the areas of aerodynamics (e.g., Menter, 1994; Bardina et al., 1997; Walsh and Leong, 2004; Cheng-Hu et al., 2005; Zhai et al., 2007; Baxevanou and Fidaros, 2008; El-Behery and Hamed, 2011; Sagol et al., 2012; Heschl et al.,2013). However, few studies have been conducted to investigate the effectivity of various turbulence models in simulating two-phase pipeline flow. Banerjee and Isaac (2003) evaluated three turbulence models, including the standard k-ε, the RNG k-ε and the Reynolds stress model, in conjunction with the volume of fluid (VOF) multiphase flow model with FLUENT in predicting stratified gas-liquid flow. They found that the RNG k-ε model provided better predictions. Vallée et al. (2008) used the SST k-ω model to simulate gas-liquid slug flow in conjunction with the inhomogeneous multiphase model with CFX; the interface turbulence damping function was applied for the SST

k-ω model. A very good qualitative agreement between calculation and experiment was demonstrated. Walvelar et al. (2009) simulated dispersed oil-water pipeline flow with FLUENT. The Eulerian-Eulerian method and the standard *k-ε* turbulence model were used. The predicted results were satisfactory at high mixture velocity, while at low mixture velocity, the authors observed notable discrepancy to the data. Burlutskiy and Turangan (2015) investigated dispersed oil in water in a vertical pipe using a steady Euler-Lagrange model and a *k-ε* turbulence model implemented in FLUENT. The predictions for pressure drop were satisfactory at high mixture velocity, and the authors highlighted the importance of the shear-lift force on their prediction. With respect to core annular flow that is a subject of the present work, simulations have been performed with the VOF model for flow through various line configurations. Ghosh et al. (2010) numerically simulated downward CAF (oil-to-water viscosity ratio 220) in a small and short vertical pipe (I.D.=0.012 m, pipe length=0.48 m). The standard *k-ε* turbulence scheme was used for turbulent flow conditions. A good agreement was shown between calculation and experiment. The simulation results showed an abrupt change in the radial velocity gradient at the phase interface with velocity across the oil core being roughly flat. Though the calculated liquid hold-up showed little variation at a specific distance downstream (22 times the pipe diameter), the velocity profiles still showed variation at that specific distance downstream, indicating the calculated flow is unlikely fully developed in the simulations described above. Ghosh et al. (2011) further performed simulations of CAF (oil-to-water viscosity ratio 220) in a vertical U bend with the same CFD models as used in their previous study (Ghosh et al., 2010). The simulation results showed a satisfactory agreement with experiments concerning liquid distributions. Core annular flow through sudden contraction and expansion were investigated in Kaushik et al. (2012). The authors also applied the standard *k-ε* turbulence scheme for turbulent annulus flow. The authors observed that an increase in the superficial velocity of the annulus prevents from fouling. Jiang et al. (2014) also investigated CAF through a U bend configuration with the Eulerian-Eulerian approach and compared simulation results with that from VOF approach reported by Ghosh et al. (2010). The study showed that there is no major discrepancy between the two approaches.

In general, applications of the VOF modeling of liquid-liquid two-phase flow in the literature as introduced above concern simulations of a particular flow regime within the category of separated flow, such as stratified flow, slug flow or core annular flow. For turbulent liquid-liquid flow, the standard k-ε turbulence scheme is popularly used without evaluation of different turbulence models. Also, most of the existing CFD studies on liquid-liquid pipeline flow in the literature as reviewed above seldom give attention to the selection of wall contact angle. In addition, CAF with relatively low viscosity has received little attention though high-viscosity oil CAF has been extensively studied. The aim of the current work is to examine the capability of the VOF model to simulate horizontal oil-water two-phase flow with matched density and medium viscosity ratio under flow rates corresponding to different flow patterns, namely, core annular flow, oil plugs in water, oil bubbles in water, and dispersed flow. One the one hand, this study includes investigation on effectiveness of several turbulent models as well as the influence of the wall contact angle for the simulation of oil-water pipeline flow when the interfacial tension and/or the inertia play more prevailing roles. On the other hand, the flow characteristics of CAF with relatively low-viscosity oil (16.8 cP) is highlighted based on the simulation results. In the present study, we utilized the commercial CFD package FLUETN to perform the simulations. The validation was achieved via the acknowledged experimental work of Charles et al. (1961). A literature survey shows that this is the only experimental study on oil-water pipeline flow with matched density and medium viscosity ratio in the literature. The paper is structured as follows. Descriptions of the CFD models and the simulation setup are presented in Section 2. The simulation results and discussion are presented in Section 3. Conclusions are summarized in Section 4.

2. CFD model and simulation setup

2.1 Mathematical model description

2.1.1 VOF model

In the VOF model, a single set of conservation equations is shared by the phases. Considering an isothermal system with no mass transfer and no phase change, the conservation equations are:

Mass equation: $\frac{\partial(\rho)}{\partial t}+\nabla\cdot(\rho\mathbf{u})=0$ (1)

Momentum equation: $\frac{\partial}{\partial t}(\rho\mathbf{u})+\nabla\cdot(\rho\mathbf{u}\cdot\mathbf{u})=-\nabla p+\nabla\cdot\left[\mu\left(\nabla\mathbf{u}+\nabla\mathbf{u}^{T}\right)\right]+\rho\mathbf{g}+\mathbf{F}$ (2)

The interface between the water phase (primary) and the oil phase (secondary) is tracked by solving the conservation equation for the volume fraction of the secondary phase (oil), α_o

$\frac{\partial(\rho_o\alpha_o)}{\partial t}+\nabla\cdot(\rho_o\alpha_o\mathbf{u})=0$ (3)

The volume fraction of the primary phase (water) is determined by the constraint

$\alpha_w+\alpha_o=1$ (4)

The phase volume fraction has a value of 0 or 1 when a control volume is entirely filled with oil or water, and a value between 0 and 1 if an interface is present in the control volume.

Material properties in the transport equations are determined by the presence of the component phases in each control volume. Considering ideal mixtures, i.e., the mixture has a volume equal to the sum of the volumes of the individual components, the density of the oil-water mixture in each cell is

$\rho=\alpha_o\rho_o+\alpha_w\rho_w$ (5)

There is no universal theory for the calculation of the viscosity of mixture from viscosities of individual components. The simplified linear combination is used for the calculation of the mixture viscosity

$\mu=\alpha_o\mu_o+\alpha_w\mu$ (6)

The term $\mathbf{F}$ in the momentum equation stands for the contribution of surface tension. The continuum surface force (CSF) model proposed by Brackbill et al. (1992) was used. It is dependent on the surface tension coefficient, σ, and the curvature of the interface, κ

$\mathbf{F}=\sigma\kappa\frac{\rho\nabla\alpha_0}{\frac{1}{2}(\rho_w+\rho_o)}$ (7)

The curvature, κ, is defined in terms of the divergence of the unit normal, $\hat{\mathbf{n}}$

$\kappa=\nabla\cdot\hat{\mathbf{n}}$ (8)

$$\hat{\mathbf{n}} = \frac{\mathbf{n}}{|n|} \tag{9}$$

where $\mathbf{n}$ is the surface normal, defined as the gradient of the volume fraction of the oil phase, α_o

$$\mathbf{n} = \nabla \alpha_o \tag{10}$$

The effect of wall adhesion at fluids interfaces in contact with rigid boundaries is modelled within the framework of the CSF model. The unit surface normal at the live cell next to the wall is replaced by the following equation, which is the so-called dynamic boundary condition, resulting in adjustment of the curvature of the surface near the wall:

$$\hat{\mathbf{n}} = \hat{\mathbf{n}}_{wl} \cos\theta_{wl} + \hat{\mathbf{t}}_{wl} \sin\theta_{wl} \tag{11}$$

where $\hat{\mathbf{n}}_{wl}$ and $\hat{\mathbf{t}}_{wl}$ are the unit vectors normal and tangential to the wall, respectively. The contact angle, θ_{wl}, is the angle between the wall and the tangent to the interface at the wall.

2.1.2 SST k-ω turbulence model

The choice of turbulence model is crucial for turbulent two-phase flow modeling. The family of *k-ε* models is very popular for industrial applications due to its good convergence rate and relatively low memory requirement. The large number of examples in the literature also contributes to its popularity. Another family of two-equation eddy viscosity models is *k-ω* models. The shear stress transport (SST) *k-ω* scheme utilizes the original *k-ω* model of Wilcox (1998) in the inner region of the boundary layer and switches to the standard *k-ε* model in the outer region of the boundary layer and in free shear flows. It has been reported that turbulence damping at the interface is necessary to predict correct pressure losses and phase holdups (Egorov, 2004; Vallée et al., 2008; Lo and Tomasello, 2010). As turbulence damping at the interface can be included in the SST k-ω turbulence model in FLUENT, the SST *k-ω* model was used in the present study.

The governing equations of the SST *k-ω* model are:

Turbulent kinetic energy: $$\frac{\partial(\rho k)}{\partial t} + \nabla \cdot (\rho k \mathbf{u}) = \nabla \cdot \left(\left(\mu + \frac{\mu_t}{\sigma_k} \right) \nabla \cdot k \right) + G_k - Y_k \tag{12}$$

Specific dissipation rate*:*
$$\frac{\partial(\rho\omega)}{\partial t}+\nabla\cdot(\rho\omega\mathbf{u})=\nabla\cdot\left(\left(\mu+\frac{\mu_t}{\sigma_\omega}\right)\nabla\cdot\omega\right)+G_\omega-Y_\omega+D_\omega \quad (13)$$

where G_k , G_ω represent the generation of k and ω , respectively; Y_k , Y_ω represent the dissipation of k and ω , respectively; D_ω represents the cross-diffusion term; μ_t represents the turbulent viscosity, $\mu_t=\frac{\rho k}{\omega}$. More information on the formulation for these quantities can be found in Wilcox (1988), Menter (1994) or Fluent theory guide (2012).

When the turbulence damping option is activated in FLUENT, an additional source term first suggested by Egorov (2004) is added to the *ω*-equation for reduction of the destruction term. This additional source term is expressed as

$$S_\omega=A_i\Delta n\beta\rho_i\omega_\omega^2 \quad (14)$$

$$\omega_\omega=B\frac{6\mu_i}{\beta\rho_i\Delta n^2} \quad (15)$$

$$A_i=2\alpha_i\left|\nabla\alpha_i\right| \quad (16)$$

where A_i represents an interface area density that activates the correction term in the vicinity of the interface only (A_i =0 outside the interface region); α_i is the volume fraction of phase i ; Δn is the grid size in the interface region; β is a closure coefficient, β =0.075; B is a damping factor which can be specified, the default value is 10. This additional source term is mesh size dependent (through Δn). The tunable parameter B is an empirical coefficient which was obtained through numerical experiments (Egorov, 2004).

The popular *k-ε* models were also tested in this study to investigate the effectiveness of turbulence models. The formulation of different *k-ε* models can be found in Fluent theory guide (2012).

2.2 Physical problem description

The facility for the numerical study is depicted in Fig. 1. The pipe diameter, *d*, is 0.026 m, the length downstream of the junction is 4 m (154 *d*), and the length of each branch of the junction is 0.2 m. Fig. 2 shows a partial view of the mesh at the water inlet. The mesh is progressively

finer near the pipe wall. A mesh independence study was conducted to ensure the integrity of the solution from the mesh resolution. The final mesh used for the present simulations consists of about 1.2 million cells.

2.3 Boundary and initial conditions

The outlet pressure was applied at the outlet; a gauge pressure of zero, i.e., the atmospheric pressure, was specified at the outlet. No-slip boundary condition was imposed at the wall. The wall contact angle in the wall adhesion modeling (see Eq. 11) was specified as a boundary condition. A contact angle of 175° was used in the present study; different contact angles have been tested as discussed in the following section 3.2. Velocity inlet boundary was set up at the inlets. For the purpose of saving computation time, instead of using a uniform velocity and a longer pipe length to achieve fully developed single phase flow before the junction, the developed velocity profiles of single phase oil and water were coded and loaded into the solver to make sure the fluids are fully developed before the junction. As the viscosity of the oil used in the present study is 16.8 cP, the single oil flow introduced is always laminar with Reynolds number lower than 2 000. The single water flow is either laminar or turbulent depending on the Reynolds number. The velocity profiles for single phase laminar flow and turbulent flow are:

Laminar flow: $$f(r) = 2U\left(1 - \frac{r^2}{R^2}\right) \tag{17}$$

Turbulent flow: $$f(r) = \frac{(m+1)(2m+1)}{2m^2} U\left(1 - \frac{r}{R}\right)^{1/m} \tag{18}$$

where *U* represents the average velocity, r the radial position in the circular section, R the radius of the pipe. For the velocity profile of turbulent flow, *m* is an empirical coefficient determined from the range of Reynolds number (see Schlichting, 1979).

Apart from the velocity, the turbulence intensity and hydraulic diameter were specified when the turbulence model was used. The turbulence intensity at the core of a fully-developed duct flow is estimated through

$$\mathrm{I} = 0.16\mathrm{Re}^{-1/8} \tag{19}$$

2.4. Solution setup

Calculations were conducted with flow conditions from experiments of Charles et al. (1961). Five flow regimes, namely water drops in oil, core annular flow, oil plugs in water, oil bubbles in water, and oil drops in water, are covered. No stratified flow was observed as carbon tetrachloride was used to alter the density of oil to match that of water in the experiments of the above authors.

Material properties were set up the same as those in the experiments: both oil and water have a density of 998 kg m^{-3}; the viscosity of oil is 16.8 cP and the viscosity of water is 0.894 cP; the interfacial tension is 0.045 N m^{-1}.

The problem was solved as a transient flow. The explicit VOF scheme was used. Whether the flow was solved as laminar flow or turbulent flow depends on the flow conditions. The water flow rates determine whether the turbulence model would be activated or not since the oil phase is laminar due to its relatively high viscosity. For core annular flow, the Reynolds number of the annular water film can be calculated as

$$\mathrm{Re}_w = \frac{\rho_w U_w d_{we}}{\mu_w} \tag{20}$$

$$D_{we} = \frac{4A_w}{\pi \mathrm{d}} = H_w \mathrm{d} \tag{21}$$

$$U_w = \frac{U_{sw}}{H_w} \tag{22}$$

where d_{we} represents the hydraulic diameter, U_w the film average velocity, A_w the cross-sectional area occupied by water ($A_w = AH_w$), H_w the water holdup ($H_w = A_w/A$, A the cross-sectional area of the pipe), U_{sw} the superficial water velocity. Substituting Eqs. (21) and (22) into Eq. (20) yields

$$\mathrm{Re}_w = \mathrm{Re}_{sw} = \frac{\rho_w U_{sw} d}{\mu_w} \tag{23}$$

In the present study, the flow was solved as laminar when $\mathrm{Re}_{sw} < 2\,300$. Laminar condition was applied for three cases with Re_w=778 and SST *k-ω* turbulence model was applied for seven cases with Re_w of 6331 and 14271.

The simulation domain was initialized with the water inlet flow conditions. The pressure-based segregated algorithm was used to solve the transport equations. The PRESTO! (pressure staggering option) scheme was used for the pressure interpolation. The SIMPLE

(semi-implicit method for pressure linked equations) scheme was used for the pressure-velocity coupling. First-order upwind spatial discretization scheme for momentum equation was applied first and switched to second-order upwind scheme after convergence could be easily achieved after some time of run. The Geo-Reconstruct scheme was used to determine the interface shape. A smaller time step in the magnitude of 10^{-5} s was used first to obtain convergence and later increased to the magnitude between10^{-4} and 10^{-3} s at which the global Courant number was around 0.6~0.8. Convergence was judged based on transport equation residuals; absolute criteria were set at 10^{-6} for the transport equations. Average static pressures and water volume fractions at various cross sections were monitored. Each simulation case was run until the monitored values have reached a stable solution for enough sampling time. With 32 processors of 2 nodes (each node has two eight-core 2.6GHz Xeon CPUs and 64GB RAM) from a cluster used for each case, the CPU time used was around 2 to 5 days for a simulation time of around 25 s.

3. Results and discussion

3.1 Influence of turbulence scheme

An investigation of two-equation turbulence models has been conducted with the standard *k-ε*, RNG *k-ε* and SST *k-ω* with and without turbulence damping in conjunction with the VOF model to simulate oil-water flow for Case 9 (U_{sw}=0.55 m s^{-1}, and U_{so}=0.55 m s^{-1}). The enhanced wall treatment is applied for the two *k-ε* models. In all simulations, the near wall grids have a y+ <5.

Flow patterns predicted from the VOF model in conjunction with different turbulence schemes are displayed in Fig. 3. As illustrated in the color map, the red represents the oil phase (α_o=1), the blue represents the water phase (α_o=0), while the other colors in between represent the cells containing the interface where the volume fraction of the oil phase varies (0< α_o <1). For all the following figures in this paper which illustrate the distribution of phases, the color map shown in Fig.3 applies. The corresponding experimental flow regime can be found in Fig. 7 with the mark of '9-exp.'. It is demonstrated that the VOF model with different turbulence schemes all successfully predict core annular flow. With regard to the pressure gradient, the standard *k-ε*, RNG *k-ε* and SST *k-ω* without turbulence damping all predict higher values than the

experimental measured value, with relative errors of +21%, +19%, and +16% respectively. A closer prediction with relative error of -11% is given from the SST *k-ω* scheme with the turbulence damping function activated.

Cross-sectional turbulence characteristics obtained from different turbulence schemes are shown in Fig. 4. Turbulence properties calculated with the standard *k-ε* and RNG *k-ε* schemes are similar. The magnitudes of turbulence characteristics from these schemes exhibit comparable intensities. The magnitudes of turbulence properties calculated with the SST *k-ω* scheme without turbulence damping are slightly smaller than those predicted with the *k-ε* schemes, but still they are of same order. The cross-sectional distributions calculated with the SST *k-ω* scheme with the turbulence damping activated differ from those obtained with all the other three schemes, especially in the region near the interface of the oil and water. The turbulence intensity distribution matches the phase distribution, and similarly for the turbulent viscosity and effective viscosity. The magnitudes of turbulence characteristics obtained are nearly one order lower than those obtained with other schemes (the standard *k-ε*, RNG *k-ε*, and SST *k-ω* scheme without turbulence damping). The lower turbulence intensity from the SST *k-ω* model with turbulence damping is attributed to the additional source term (Eq. (14)) added to the *ω*-equation. Compared to the case calculated with SST *k-ω* scheme without turbulence damping, the calculated *ω* from the same scheme with turbulence damping is higher, leading to a lower turbulent viscosity ($\mu_t \approx \frac{\rho k}{\omega}$). When no special treatment of turbulence at the interface is included, the turbulent viscosities from the standard *k-ε* and RNG *k-ε* models are thought to be over predicted, which leads to the overestimated pressure gradients. The results confirm that including the turbulence damping at the interface can improve the quantitative prediction of turbulence models as reported by Vallée et al. (2008) and Lo and Tomasello (2010).

3.2 Influence of wall contact angle

Fig. 5 illustrates three scenarios of which an oil drop is surrounded by water on a solid surface. On a water-wet surface, the oil drop beads up, minimizing its contact with the solid (see Fig. 5 (a)). On an oil-wet surface, the oil drop spreads, resulting in a contact angle of about 180º

(see Fig. 5 (c)). When the condition is neither strongly water-wetting nor oil-wetting, the balance of forces in the oil/water/solid system will result in a contact angle, θ, between the fluids at the solid surface (see Fig. 5 (b)). When the force balance is out of equilibrium, the contact line will move towards its equilibrium position. The contact line motion induces an apparent dynamic (time-dependent) contact angle (Van Mourik et al., 2005). For liquid moving quickly over a surface, the contact angle can be altered from its value at rest.

An option to specify a wall adhesion angle in conjunction with the surface tension model is available in the VOF model (see Eq. (11)). The input can be either a static value or dynamic contact angle defined with UDF (User Defined Functions). The modeling of dynamic contact angle is not well established yet. Existing models are empirically based and most of the experiments only cover small Capillary numbers (Ca<0.03), thus the models based on those experiments are not generally valid (Van Mourik et al., 2005). A constant wall contact angle was used and tested in this study. It is worth remarking that the contact angle that the fluid is assumed to make with the wall is used to adjust the surface normal in cells near the wall. This so-called dynamic boundary condition results in the adjustment of the curvature of the surface near the wall. A constant contact angle does not mean that the liquid at the boundary will not move. The liquid will move towards its equilibrium position induced by a pressure correction each time step.

As no oil fouling on the pipe was observed in the experiments of Charles et al. (1961), indicating rare oil contact with the wall, an angle close to 180° is thought to be appropriate. Simulation runs were conducted to investigate the sensitivity of the simulation results to the wall contact angles for the cases studied in the present study. For an experimental core annular flow under flow conditions of U_{sw}=0.03 m s^{-1}, and U_{so}=0.15 m s^{-1}, simulations were performed with wall contact angles of 5°, 60°, 90°, 120°, 150°, and 175°, respectively.

Fig. 6 shows the contours of oil volume fractions from simulations with the different wall contact angles. The flow regime of water-core in annular oil is predicted with a very small wall contact angle of 5° (i.e., strongly oil-wetting wall). Dispersed water plugs/bubbles in continuous oil is predicted with a contact angles of 60°. An intermittent flow regime featured with water plugs/bubbles inside water alternating with partial contact of water plugs/bubbles with the pipe

wall is predicted for a contact angle of 90°, and the flow regime develops into one characterized with dual-continuous streams moving forward spirally for a wall contact angle of 120°. The flow regime of oil-core in annular water flow is predicted with large wall contact angles of 150° and 175° (i.e., strongly water-wetting wall). The experimental flow regime is core annular flow (referring the sub-image marked with '3-exp.' in Fig. 7). As anticipated, a large wall contact angle which indicates strong water-wetting wall is demonstrated to give good prediction for the case under consideration. A contact angle of 175° was used in the following simulations.

The above simulations demonstrate the sensitivity of the simulation results to the wall contact angles for the case under consideration, i.e., oil-water flow with matched density and medium viscosity ratio (μ_o/μ_w=18.8). The simulation results under different wall contact angles are thought to be reasonable. For the case under consideration, the flow is largely influenced by the interfacial tension as the influence of the gravity disappear due to matched density and the influence of the viscous force is not significant. It is noted that the influence of the interfacial tension would be reduced when the oil viscosity is significantly higher than the water viscosity (i.e., high Capillary numbers, $\mathrm{Ca} = \frac{\mu U}{\sigma}$). This can explain the fact that core annular flow has been observed to be the dominant flow regime in either hydrophobic or hydrophilic pipelines (e.g., McKibben et al., 2000a and 2000b; Al-Awadi, 2011; Sridhar et al., 2011; and Shi and Yeung, 2016). Another interesting aspect from the above simulation results is the predicted flow regimes of swirling oil and water streams before the formation of core annular flow. This kind of phase configuration has been observed in experiments on high-viscosity oil-water flow by Al-Awadi (2011).

3.3 Comparison of simulation results with experimental data

A comparison of experimental and predicted flow patterns is displayed in Fig. 7. The flow map and the illustrations of experimental flow patterns are adapted from Charles et al. (1961); for cases 6, 8 and 10, illustrations of the experimental flow patterns are not available. The results show that the flow patterns predicted from the CFD models are in good agreement with experimental flow patterns for core annular flow, oil plugs in water and oil bubbles in water. However, concerning dispersed flow (droplets of one phase in another), a clear disagreement between phase configurations is shown. The inaccuracy of the VOF approach in modeling

dispersed flow is due to the fact that the interface length scales are becoming much smaller than the computational grid size, thus the interface cannot be correctly captured. The computational grid scale along the flow direction is around 2.5 mm in this study. The sizes of visible small drops in experiments should also be around the magnitude of millimeter. A finer grid is essential to capture such small dispersed drops with the VOF model in a 4m long pipe, which implies much more expensive computation. The Mixture model, Eulerian-Eulerian, or Euler-Lagrange schemes are normally used for dispersed flow simulation (e.g., Walvelar et al., 2009; Burlutskiy and Turangan, 2015). The VOF model is more suitable for modeling immiscible fluids with interface length scale comparable or larger to the pipe diameter.

Table 1 shows comparison of pressure gradients and in situ water holdups obtained from experiments with their corresponding CFD predictions for core annular flow, oil plugs in water and oil bubbles in water flow. Dispersed flow cases are not included given the deficiency of qualitative predictions. Quantitative agreement between predictions and experiments varied by as much as 30% for the pressure gradient and 14% for the holdup. It should be noted that for Case 3 where the largest discrepancy of the pressure gradient is shown, the uncertainty in the measured pressure gradient (from 34 to 41 Pa m^{-1}) suggests that the validation of this case cannot be evaluated accurately.

3.4 Characterization of core annular flow

Analysis of fully established flows can begin when statistically steady solutions are reached. To that end, face average pressures of various sections along the pipe are monitored. Fig. 8 shows monitored average pressure at different positions along the pipe after the intersection (z=0) for two annular flow cases. As shown, statistically steady solutions are reached after some simulation time depending on flow conditions.

Fig. 9 shows the flow development of annular flow after a T-shaped junction. It illustrates the migration of oil into the central part of the pipe (core flow) and in the meantime, evacuating water to peripheral regions of the pipe to form the annulus flow. Fig. 9 also shows that when the water coming through one branch of the junction becomes turbulent, there is unsteady variation on phase distribution just after the junction and the amplitude of the variation is gradually reduced downstream.

To investigate the flow characteristics of fully established annular flow, phase distributions and dimensionless velocity profiles at different positions downstream the junction are illustrated in Fig. 10. The laminar case in Fig. 10 (a) shows a perfect CAF with established velocity profile at a distance of 20d downstream the junction. For turbulent cases shown in Fig. 10 (b) and (c), the volume fraction of the oil phase varies along the flow direction, reflecting the fluctuation of the oil core. For the cases under consideration, the two-phase flow can be regarded as fully developed beyond a distance of 40 times the pipe diameter from the junction where the U_{max}/U_m is almost constant. The velocity profile of fully developed core annular flow in Fig. 10 is different from that of the single phase flow. For the laminar CAF case shown in Fig. 10 (a), the velocity profile is radically different from the parabolic velocity distribution of single phase laminar flow. The velocity gradient of the water ring near the pipe wall becomes greater while the velocity distribution of the oil core in the middle of the tube is much flatter. For single phase laminar flow $U_{max}/U_m=2$ while it is shown that $U_{max}/U_m=1.26$ for the laminar core annular flow under consideration. For turbulent cases shown in Fig. 10 (b) and (c), the velocity distribution of annular flow is similar to that of turbulent single phase flow in general. There is no obvious sharp change in the velocity gradient at the interface, this is different from the velocity profiles of high-viscosity oil CAF where there is sharp change in the velocity gradient at the phase interface with velocity across the oil core being roughly flat (Ghosh et al., 2010; Shi, 2015). The core annular flow studied in the present study has an oil viscosity of 16.8 cP. When the oil viscosity is much higher than the water viscosity, it is more likely that the oil core has a flatter velocity distribution. The assumption that the oil core flows inside the water as a rigid body has been used in some analytical studies of CAF with high viscosity ratio (see Ooms et al,1984; Bai et al., 1996; Ko et al., 2002; Ooms et al., 2012). The simulation results show that the oil core of CAF cannot be treated as a rigid body when the oil viscosity is just one order higher than the water viscosity.

Fig. 11 shows turbulent kinetic energy along the vertical line on the symmetry plane of various cross-sections of developed turbulent CAF which corresponds to the phase and velocity distributions in Fig. 10 (b) and (c). The turbulent kinetic energy is the mean kinetic energy per unit mass associated with eddies in turbulent flow which indicates the turbulence strength. The

distributions of turbulent kinetic energy are reasonable in Fig. 11. It is indicated that the turbulence strength is low in the central part of pipe where the oil core flows. The oil viscosity for these cases is 16.8 cP; with this viscosity, the oil alone would flow in the pipe as laminar flow. Also, the turbulence strength is low at the pipe wall and the interface of oil and water due to turbulence damping effect from the pipe wall and the oil phase. The highest turbulent kinetic energy locates in the annular water layer close to the pipe wall. Comparing Fig. 11 (a) and (b), it shows that the turbulence strength in the annular water layer is increased with increase of the water flow rate.

4. Conclusions

Simulations of horizontal oil-water flow in different flow patterns including core annular flow, oil plugs/bubbles in water, and dispersed flow were performed with the CFD package FLUENT. The following conclusions can be withdrawn from the study:

- The VOF model in conjunction with the SST k-ω scheme with turbulence damping activated for turbulent flow is capable to predict the flow structures of core annular flow and oil plugs/bubbles in water. Quantitative agreement between predictions and experiments are achieved with relative errors within 30% for the pressure gradient and 14% for the holdup. The VOF approach is not an ideal choice for modeling dispersed flow (droplets of one phase in another) as the interface length scales tend to become smaller than the computational grid sizes.
- The wall contact angle can significantly affect the phase configurations of density-matched oil-water flow with medium viscosity ratio, or more generally speaking, fluids where the surface tension is playing a prevailing role. To obtain reasonable prediction for two-phase flow where the surface tension is playing a prevailing role, knowledge of the wall wettability and/or wall contact angle is of importance to set up CFD models appropriately.
- Detailed flow characteristics of density-matched CAF with relatively low-viscosity oil (16.8 cP) are shown. There is no sharp change in the velocity gradient at the phase interface for CAF with relatively low-viscosity oil (oil viscosity one order higher than the water viscosity). This is different from the velocity profiles of high-viscosity oil CAF(oil viscosity two to three orders higher than the water viscosity).

References

Al-Awadi, H., 2011. *Multiphase characteristics of high viscosity oil.* PhD Thesis, Cranfield:Cranfield University.

ANSYS® Fluent, Fluent Theory Guide (2012). USA: ANSYS Inc.

Banerjee, R., Isaac, K., 2003. Evaluation of Turbulence Closure Schemes for Stratified Two Phase Flow. in *ASME 2003 International Mechanical Engineering Congress and Exposition*: American Society of Mechanical Engineers. pp. 689-705.

Bardina, J., Huang, P., Coakley, T., 1997. *Turbulence Modeling Validation, Testing, and Development*. NASA Technical Memorandum 110446.

Baxevanou, C., Fidaros, D., 2008. Validation of numerical schemes and turbulence models combinations for transient flow around airfoil. *Engineering Applications of Computational Fluid Mechanics, 2*(2), pp. 208-221.

Brackbill, J., Kothe, D. B., Zemach, C., 1992. A continuum method for modeling surface tension. *Journal of computational physics, 100*(2), 335-354.

Burlutskiy, E., Turangan, C. K., 2015. A computational fluid dynamics study on oil-in-water dispersion in vertical pipe flows. *Chemical Engineering Research and Design*, 93, 48-54.

Charles, M. E., Govier, G. t., Hodgson, G., 1961. The horizontal pipeline flow of equal density oil-water mixtures. *The Canadian Journal of Chemical Engineering, 39*(1), 27-36.

Cheng-Hu, H., Kurabuchi, T., Ohba1, M., 2005. Numerical Study of Cross-Ventilation Using Two-Equation RANS. *International Journal of Ventilation, 4*(2), pp. 123-131.

Egorov, Y., 2004. *Validation of CFD Codes with PTS-Relevant Test Cases,* technical report, EVOL-ECORA-D07.

El-Behery, S. M., Hamed, M. H., 2011. A comparative study of turbulence models performance for separating flow in a planar asymmetric diffuser. *Computers & Fluids,* 44(1), pp. 248-257.

Ghosh, S., Das, G., Das, P. K., 2010. Simulation of core annular downflow through CFD—A comprehensive study. *Chemical Engineering and Processing: Process Intensification, 49*(11), 1222-1228.

Ghosh, S., Das, G., Das, P. K., 2011. Simulation of core annular in return bends—A comprehensive CFD study. *Chemical Engineering Research and Design, 89*(11), 2244-2253.

Heschl, C., Inthavong, K., Sanz, W., Tu, J., 2013. Evaluation and improvements of RANS turbulence models for linear diffuser flows. *Computers & Fluids, 71*, pp. 272-282.

Jiang, F., Wang, Y., Ou, J., Chen, C., 2014. Numerical Simulation of Oil-Water Core Annular Flow in a U-Bend Based on the Eulerian Model. *Chemical Engineering & Technology*, 37(4), 659-666.

Kaushik, V., Ghosh, S., Das, G., Das, P. K., 2012. CFD simulation of core annular flow through sudden contraction and expansion. *Journal of Petroleum Science and Engineering, 86*, 153-164.

Ko, T., Choi, H., Bai, R., Joseph, D., 2002. Finite element method simulation of turbulent wavy core–annular flows using a *k-ω* turbulence model method. *International journal of multiphase flow, 28*(7), 1205-1222.

Li, J., Renardy, Y., 2000. Numerical study of flows of two immiscible liquids at low Reynolds number. *SIAM review, 42*(3), 417-439.

Lo, S., Tomasello, A., 2010. *Recent progress in CFD modelling of multiphase flow in horizontal and near-horizontal pipes*. Paper presented at the 7th North American Conference on Multiphase Technology, Banff, Canada, 2-4 June 2010.

McKibben, M. J., Gillies, R. G., Shook, C. A., 2000a. A laboratory investigation of horizontal well heavy oil-water flows. *The Canadian Journal of Chemical Engineering*, 78(4), 743-751.

McKibben, M. J., Gillies, R. G., Shook, C. A., 2000b. Predicting pressure gradients in heavy oil-water pipelines. *The Canadian Journal of Chemical Engineering*, 78(4), 752-756.

Menter, F. R., 1994. Two-equation eddy-viscosity turbulence models for engineering applications. *AIAA journal, 32*(8), 1598-1605.

Ooms, G., Pourquie, M., Poesio, P., 2012. Numerical study of eccentric core-annular flow. *International journal of multiphase flow*, 42, 74-79.

Ooms, G., Segal, A., Van Der Wees, A., Meerhoff, R., Oliemans, R., 1984. A theoretical model for core-annular flow of a very viscous oil core and a water annulus through a horizontal pipe. *International journal of multiphase flow, 10*(1), 41-60.

Sagol, E., Reggio, M., Ilinca, A., 2012. Assessment of two-equation turbulence models and validation of the performance characteristics of an experimental wind turbine by CFD. *ISRN Mechanical Engineering, 2012*.

Schlichting H., 1979. *Boundary Layer Theory (7th Ed.):* McGraw-Hill Book Company, New York.

Shi, J., 2015. A study on high-viscoisty oil-water two-phase flow in horizontal pipes, PhD thesis, Cranfield University, Cranfield, UK 2015, p. 195-222.

Shi, J., Yeung, H., 2016. Characterization of liquid-liquid flows in horizontal pipes. *AIChE Journal*. Early online, DOI : http://dx.doi.org/10.1002/aic.15452.

Sridhar, S., Zhang, H.-q., Sarica, C., Pereyra, E. J., 2011. *Experiments and Model Assessment on High-Viscosity Oil/Water Inclined Pipe Flows*. Paper presented at the SPE Annual Technical Conference and Exhibition.

Vallée, C., Höhne, T., Prasser, H. M., & Sühnel, T., 2008. Experimental investigation and CFD simulation of horizontal stratified two-phase flow phenomena. *Nuclear Engineering and Design, 238*(3), 637-646.

Van Mourik, S., Veldman, A., Dreyer, M., 2005. Simulation of capillary flow with a dynamic contact angle. *Microgravity-Science and Technology*, 17(3), 87-93.

Walsh, P., Leong, W., 2004. Effectiveness of several turbulence models in natural convection. *International Journal of Numerical Methods for Heat & Fluid Flow, 14*(5), pp. 633-648.

Walvekar, R. G., Choong, T. S., Hussain, S., Khalid, M., Chuah, T., 2009. Numerical study of dispersed oil–water turbulent flow in horizontal tube. *Journal of Petroleum Science and Engineering, 65*(3), 123-128.

Wilcox, D. C., 1998. *Turbulence modeling for CFD (Vol. 2):*DCW industries La Canada, CA.

Zhai, Z. J., Zhang, Z., Zhang, W., Chen, Q. Y., 2007. Evaluation of various turbulence models in predicting airflow and turbulence in enclosed environments by CFD: Part 1—Summary of prevalent turbulence models. *Hvac&R Research, 13*(6), pp. 853-870.

Figure and Table Captions

Fig. 1. Geometry for oil-water flow simulation.

Fig. 2. Mesh of partial geometry (the water inlet part).

Fig. 3. Predicted flow patterns with the VOF model together with different turbulence schemes - (a) Standard *k-ε*; (b) RNG *k-ε*; (c) SST k-ω without turbulence damping; (d) SST k-ω with turbulence damping. The red represents oil and the blue represents water.

Fig. 4. Cross-sectional turbulence characteristics from different turbulence schemes - (a) Standard *k-ε*; (b) RNG *k-ε*; (c) SST k-ω without turbulence damping; (d) SST k-ω with turbulence damping.

Fig. 5. Illustration of wall wettability and wall contact angle. (a) Strongly water-wetting; (b) moderately water-wetting; (c) strongly oil wetting.

Fig. 6. Calculated flow patterns from simulations with the different wall contact angles - (a) 5°; (b) 60°; (c) 90°; (d) 120°; (e) 150°; (f) 175°. The red represents oil and the blue represents water.

Fig. 7. Comparison of experimental and CFD predicted flow patterns. Illustrations of experimental flow patterns are adapted from Charles et al. (1961); the black represents water and the white with dots inside represents oil. Illustrations of flow patterns from simulation are contours of oil volume fraction of developed flow; the red represents oil and the blue represents water.

Fig. 8. Monitored face average pressure with simulation time. (a) Case 3, Re_{sw}=778; (b) Case 9, Re_{sw}=14 271.

Fig. 9. Flow development of core annular flow after a T-shaped junction. (a) Case 3, Re_{sw}=778; (b) Case 6, Re_{sw}=6 331; (c) Case 9, Re_{sw}=14 271.

Fig. 10. Dimensionless phase distribution and velocity profiles at different distances downstream the junction. (a) Case 3, Re_{sw}=778; (b) Case 6, Re_{sw}=6 331; (c) Case 9, Re_{sw}=14 271.

Fig. 11. Turbulent kinetic energy distribution of developed turbulent CAF. (a) Case 6, Re_{sw}=6 331; (b) Case 9, Re_{sw}=14 271.

Table 1. Comparison of experimental and CFD predicted pressure gradients and in situ water holdups.

Case	Pressure gradient (Pa m^{-1})			In situ water holdup		
	Exp.	CFD	Error	Exp.	CFD	Error

Oil bubbles in water	1	10.2	9.95	-2.5%	0.7	0.677	-3.3%
	4	37.4	46.3	23.9%	0.849	0.857	0.9%
Oil plugs in water	2	15.3	18.8	22.9%	0.39	0.338	-13.6%
	5	86.6	110.5	27.6%	0.543	0.599	10.2%
	8	295.5	286.5	-3.0%	0.694	0.746	0.5%
Core annular flow	3	34 ~41	26.3	-29.9% *	0.249	0.273	9.5%
	6	244.5	198.1	-19.0%	0.403	0.445	10.4%
	9	482.2	427.0	-11.4%	0.557	0.604	8.5%

* The average experimental pressure gradient, 37.5 Pa m^{-1} , is used for the calculation of the relative error

Highlights:

- Several different turbulent models for simulating liquid-liquid flow with density-matched and medium viscosity ratio in several different flow regimes were investigated; the results demonstrated that the SST *k-ω* scheme with the interface turbulence damping option activated provides better results.
- The influence of wall contact angels for simulating density-matched oil-water flow with medium viscosity ratio (or more generally speaking, fluids where the surface tension is playing a prevailing role) was investigated; the results showed that the wall contact angle can significantly affect the phase configurations for the case investigated and highlighted the importance of selecting appropriate wall contact angles for simulating liquid-liquid flow in which the surface tension is dominant.

- CAF with relatively low-viscosity oil (oil viscosity just one order higher than the water viscosity) has not been discussed sufficiently in the literature. The simulation results showed that different from the velocity profiles of high-viscosity oil CAF where there is sharp change in the velocity gradient at the phase interface with velocity across the oil core being roughly flat, there is no sharp change in the velocity gradient at the phase interface for CAF with relatively low-viscosity oil.

Figure 1

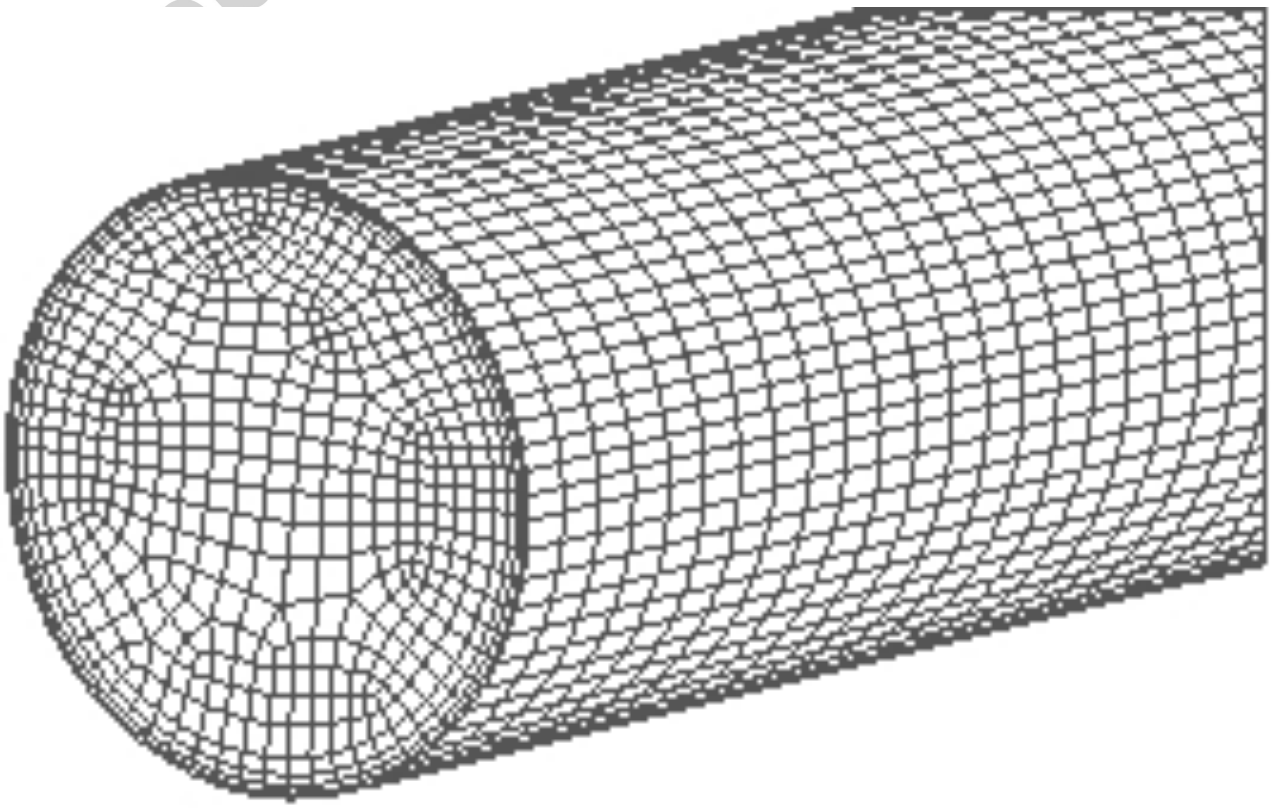

Figure 3

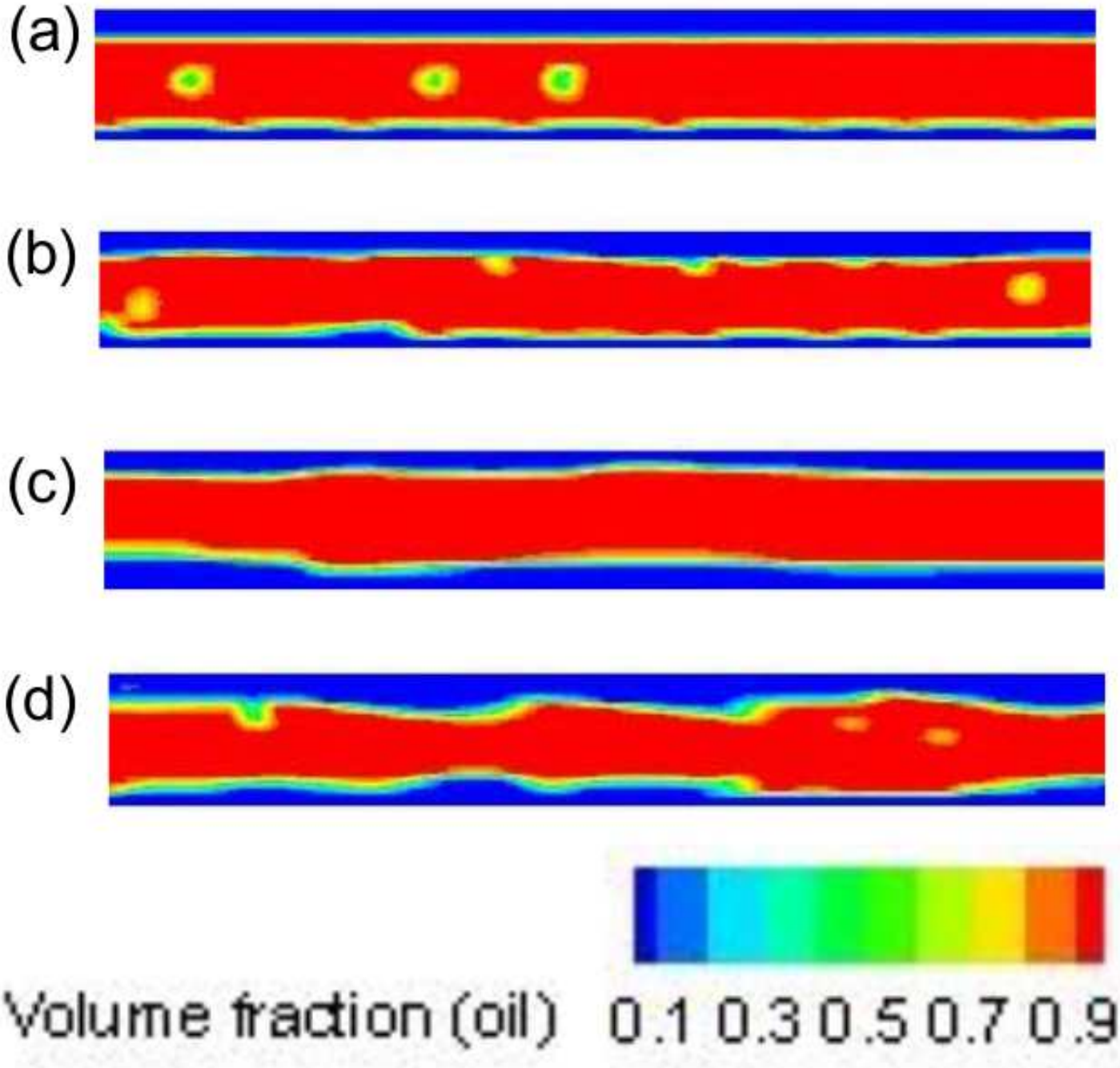

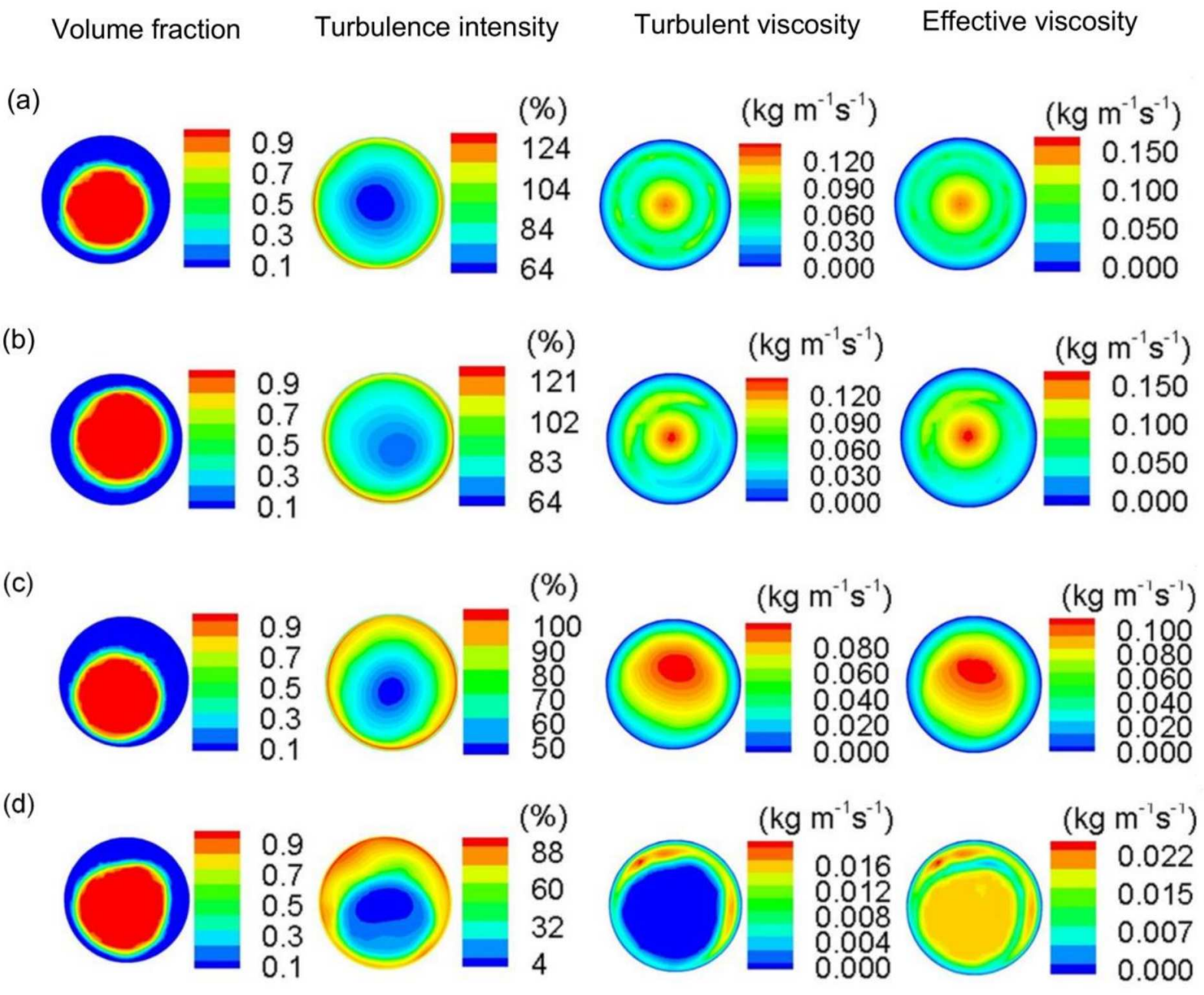

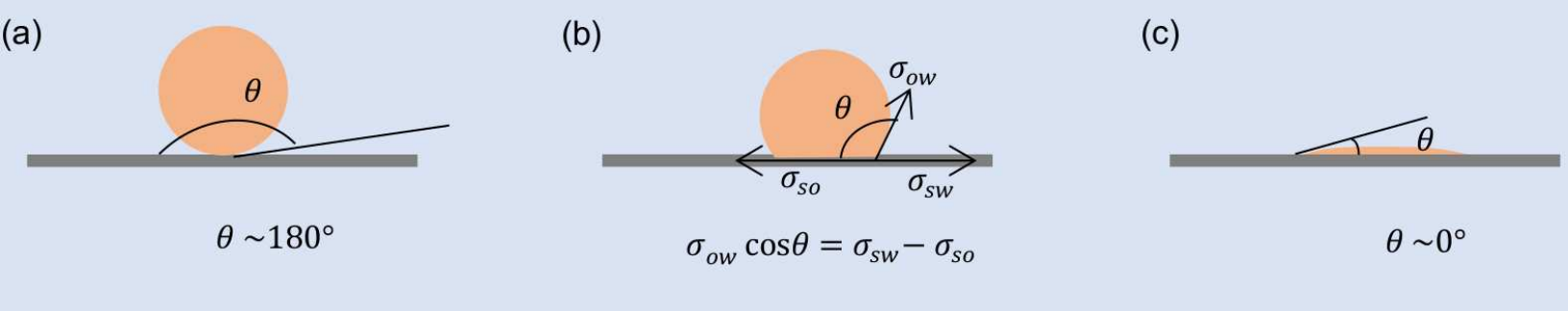

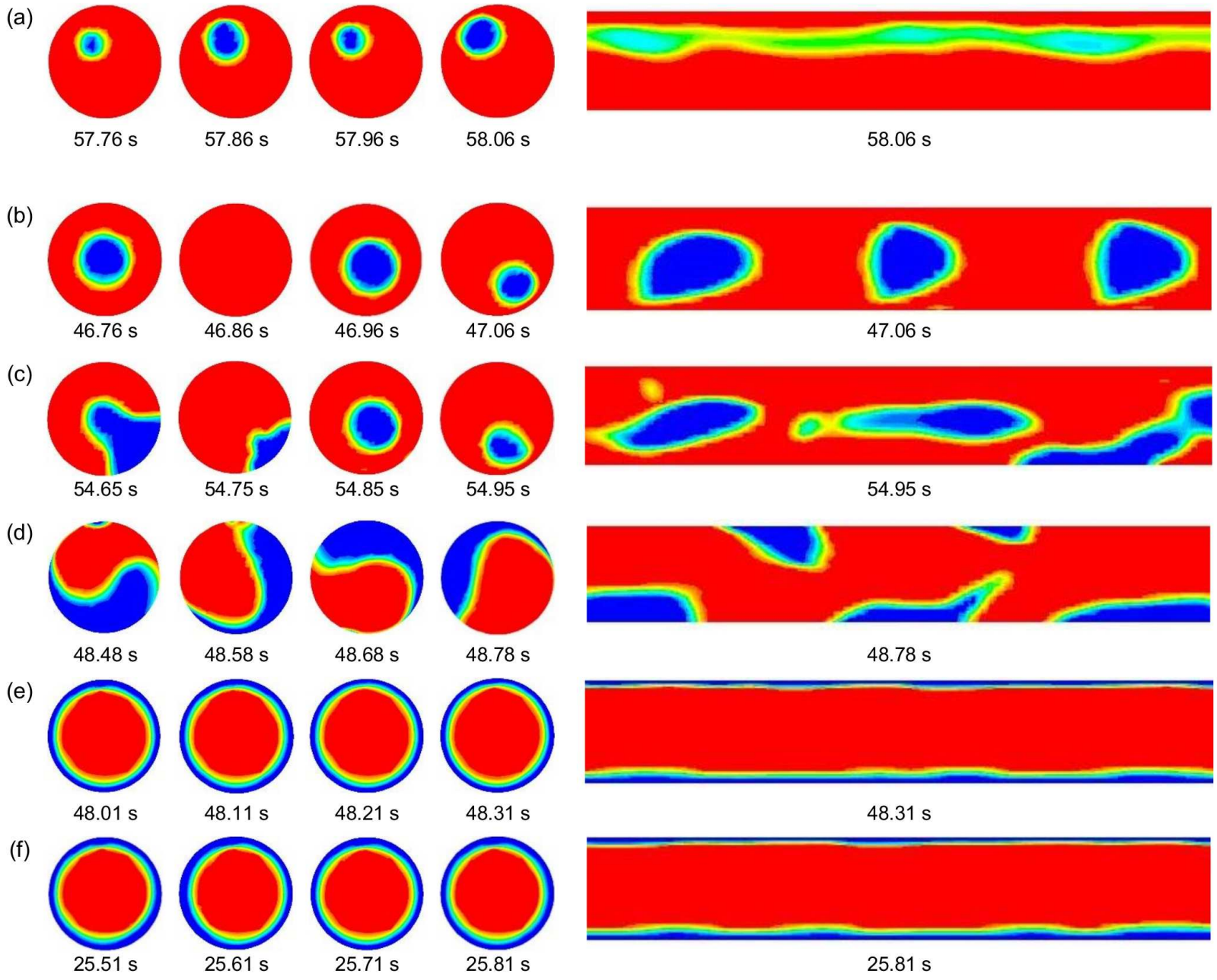

Figure 7

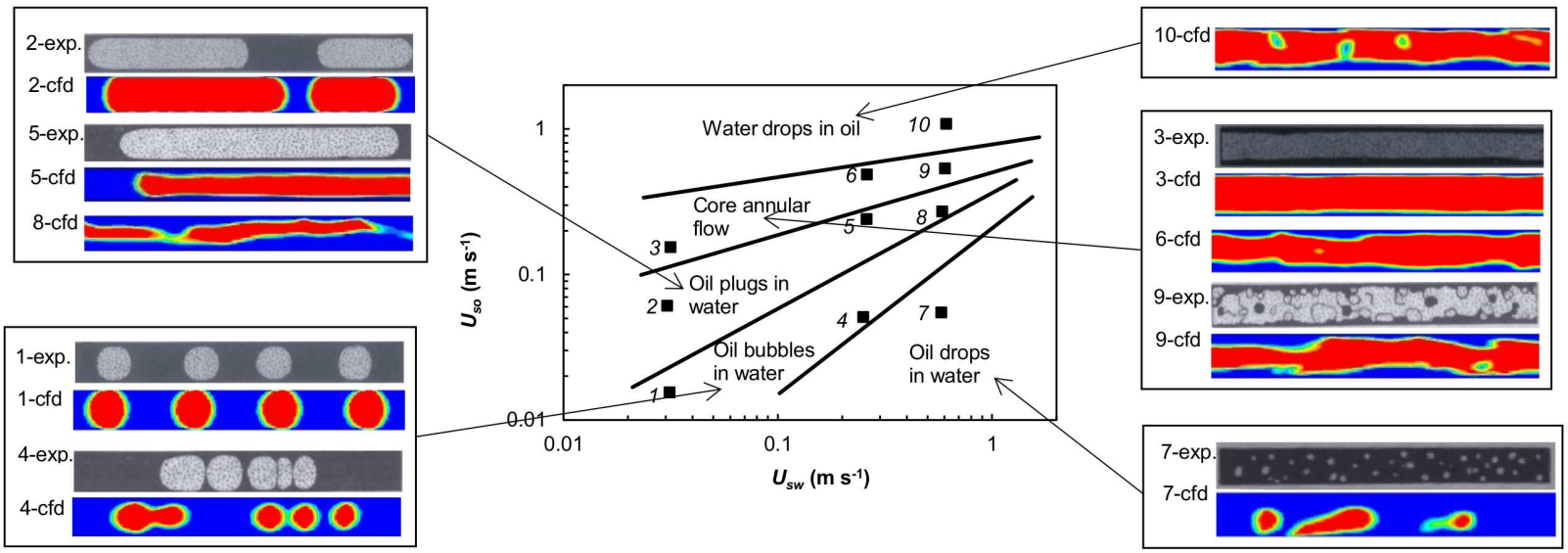

Figure 8

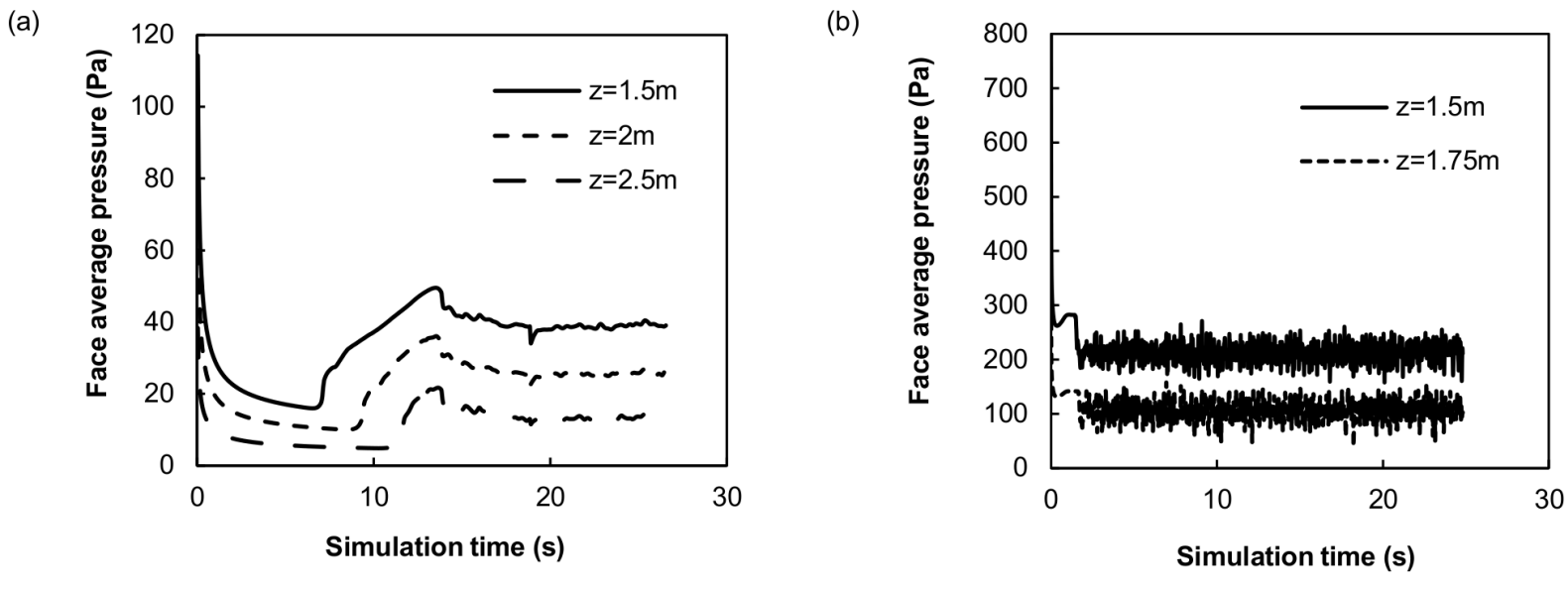

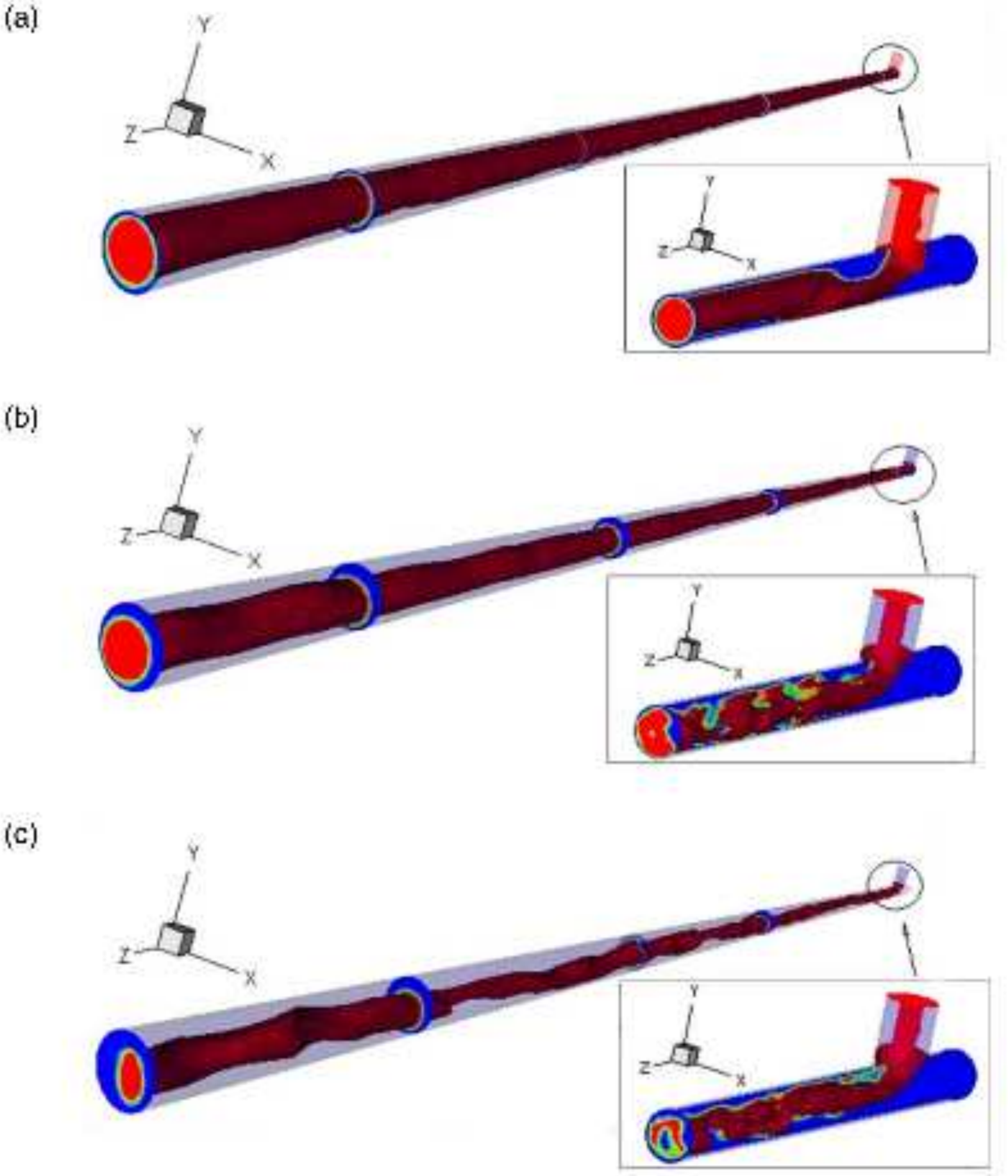

(a)

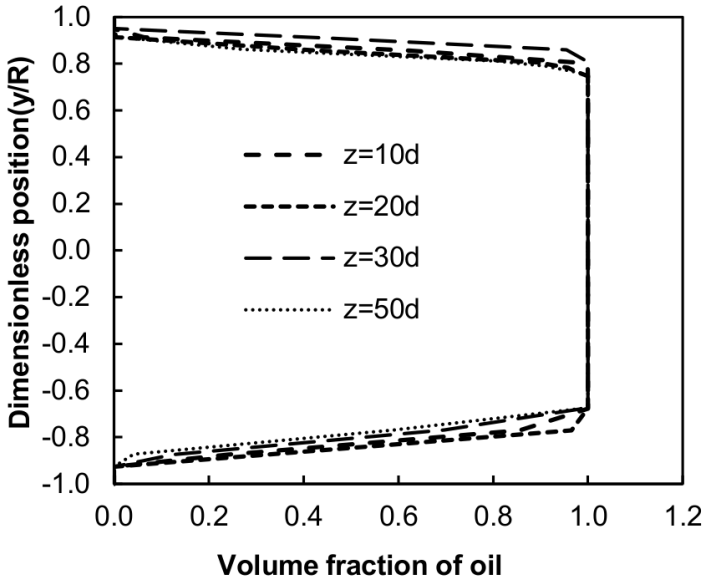

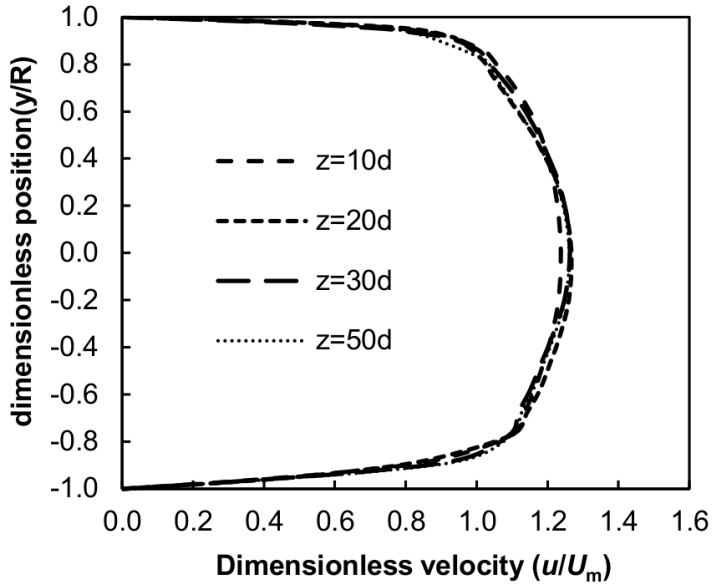

(b)

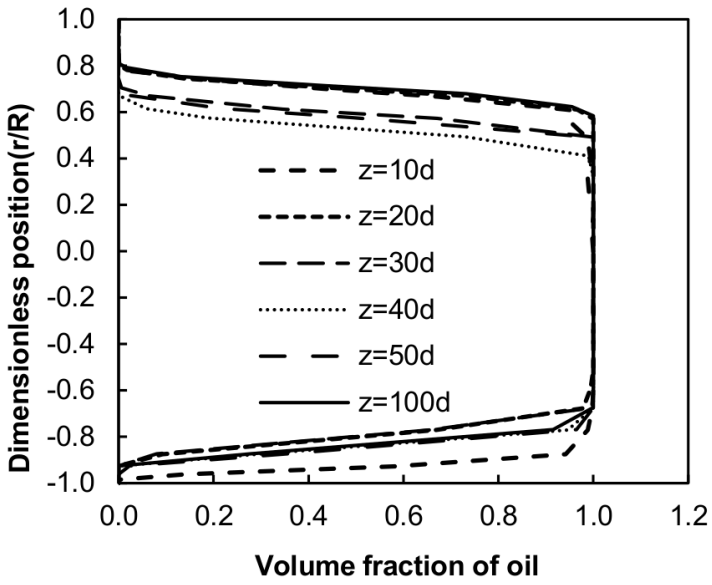

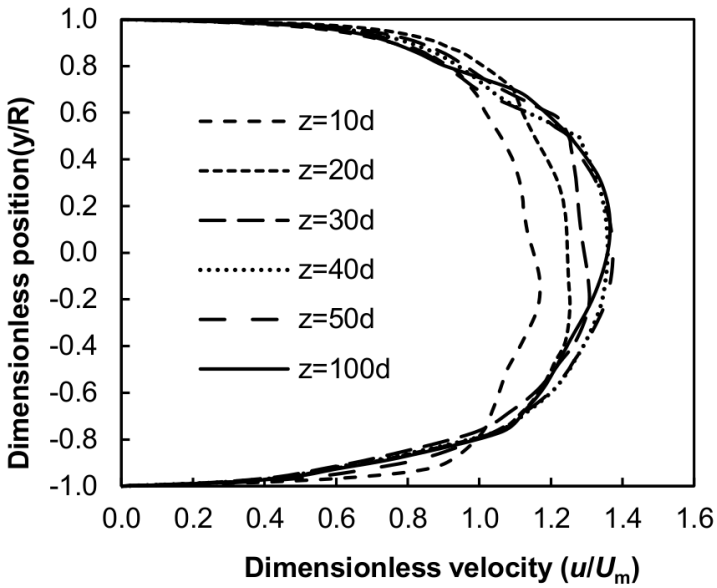

(c)

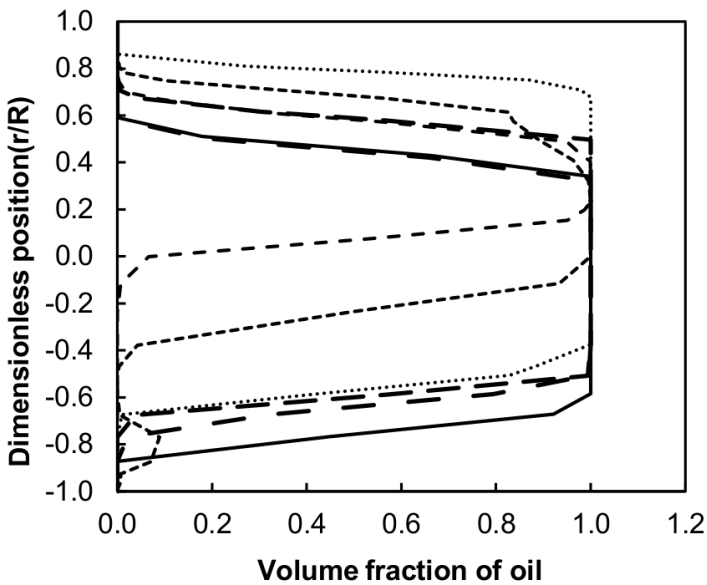

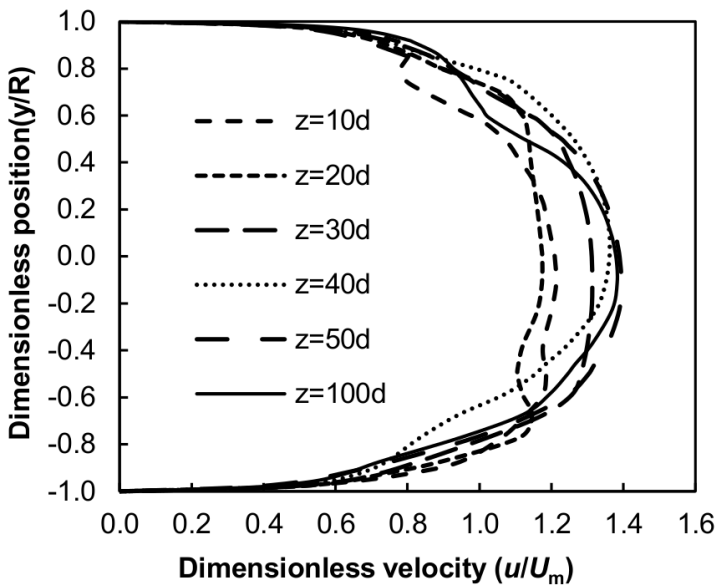

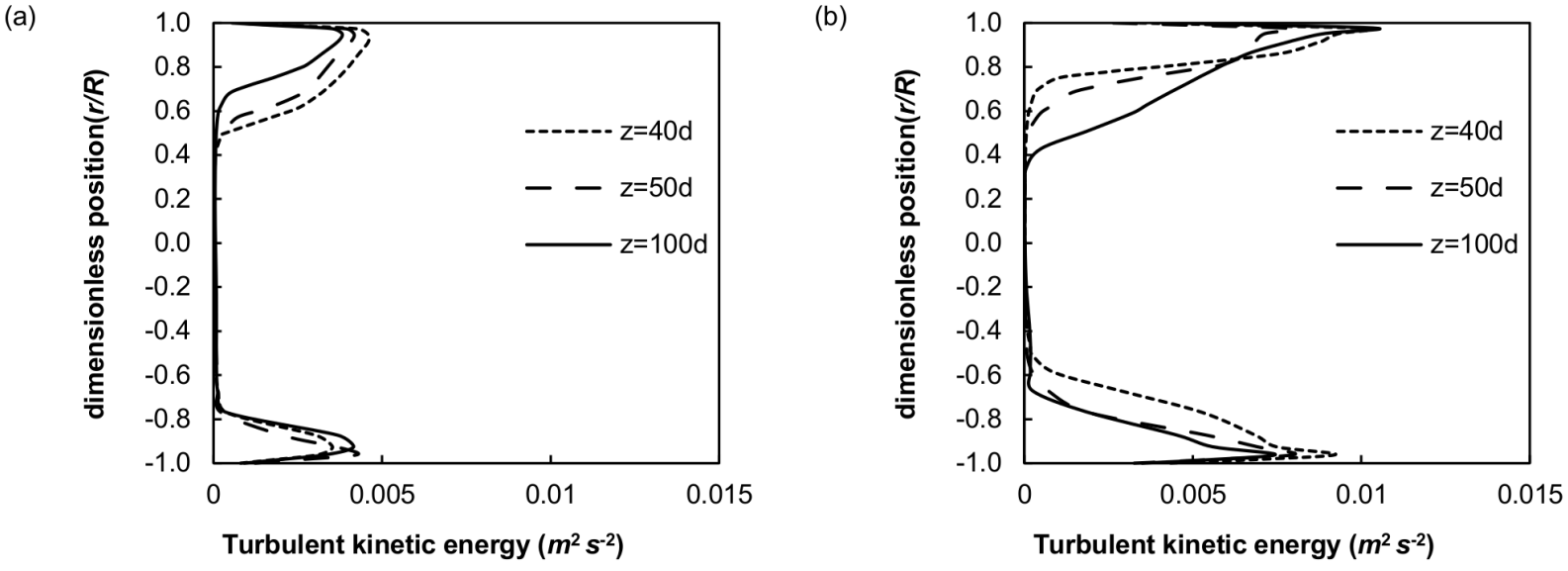

CFD simulation of horizontal oil-water flow with matched density and medium viscosity ratio in different flow regimes

Shi, Jing

2017-01-10

Jing Shi, Mustapha Gourma, Hoi Yeung, CFD simulation of horizontal oil-water flow with matched density and medium viscosity ratio in different flow regimes, Journal of Petroleum Science and Engineering, Volume 151, March 2017, Pages 373 - 383.

http://dx.doi.org/10.1016/j.petrol.2017.01.022